

# Trapping of sustained turbidity currents by intraslope minibasins

MICHAEL P. LAMB<sup>1</sup>, HORACIO TONIOLO<sup>2</sup> and GARY PARKER

*St. Anthony Falls Laboratory, University of Minnesota, Minneapolis, MN 55414, USA (E-mail: mpl@berkeley.edu)*

## ABSTRACT

Depositional turbidity currents have filled many intraslope minibasins with sediment creating targets for petroleum exploration. The dynamics of sustained turbidity currents and their depositional characteristics are investigated in a scaled physical model of a minibasin. Each turbidity current deposited a downstream thinning wedge of sediment near the inlet. Farther downstream the turbidity current was ponded by a barrier. The ponded part of the turbidity current was separated from the sediment-free water above by a relatively sharp, horizontal settling interface indicating highly Froude-subcritical flow. The very slow moving flow within the ponded zone created conditions for the passive rainout of suspended sediment onto the bed. In the lower part of the ponded zone, the concentration and mean grain-size of the sediment in suspension tended to be relatively uniform in both the vertical and streamwise directions. As a result, the deposit emplaced in the ponded zone showed only a weak tendency toward downstream fining and was passively draped over the bed in such a way that irregularities in the inerodible bed were accurately reflected. The discharge of suspended sediment overflowing the downstream end of the minibasin was significantly less than the inflow discharge, resulting in basin sediment trapping efficiencies >95%. A simple model is developed to predict the trapping of sediment within the basin based on the relative magnitudes of the input discharge of turbid water and the detrainment discharge of water across the settling interface. This model shows a limiting case in which an intraslope basin captures 100% of the sediment from a ponded turbidity current, even through a succession of sustained flow events, until sediment deposition raises the settling interface above the downstream lip of the minibasin. This same process defines one of the mechanisms for minibasin filling in nature, and, when this mechanism is operative, the trap efficiency of sediment can be expected to be high until the minibasin is substantially filled with sediment.

**Keywords** Froude number, intraslope, minibasin, ponding, turbidite, turbidity current.

## INTRODUCTION

Diapiric intraslope basins, or *minibasins*, are an important morphological feature on many contin-

Present addresses: <sup>1</sup>Earth and Planetary Sciences, University of California Berkeley, CA 94720-4767, USA.

<sup>2</sup>Department of Civil Engineering, University of Alaska, Fairbanks, AK, USA.

ental slopes. Examples include the north slope of the Gulf of Mexico (Pratson & Ryan, 1994; Badalini *et al.*, 2000; Beaubouef & Friedmann, 2000), Trinidad and Tobago (Brami *et al.*, 2000) and Angola (Schollnberger & Vail, 1999). Diapiric minibasins are formed from a buoyant instability created by loading of a less dense layer capable of flow (such as salt) by a denser layer of deposited sediment. Minibasins are of economic importance

because they are prime targets for oil exploration when filled with siliciclastic sediments. Many minibasins are believed to fill by deposition from turbidity currents through a process of fill-and-spill. The dynamics of turbidity currents within minibasins and their depositional characteristics are, however, poorly understood.

Topography can significantly affect the dynamics and deposition of turbidity currents (Kneller & Buckee, 2000). Turbidity currents that meet counter slopes can reflect creating an upstream migrating bore (Kneller *et al.*, 1991; Edwards, 1993). In minibasins, turbidity currents can pond if the downstream lip of the minibasin is high enough (on the order of the flow depth) to present an obstacle to the flow (Rottman *et al.*, 1985; Woods *et al.*, 1998), and if the duration of the flow is longer than the timescale for the upstream migrating bore to stabilize (on the order of an hour at natural minibasin scale; Lamb *et al.*, 2004). The term *ponded* in this context does not refer to the lack of overflow of the turbidity current; rather, it describes the existence of a zone of very slow-moving, highly Froude-subcritical flow within the basin, whether or not overflow occurs.

Dense underflows such as turbidity currents can be characterized by the densimetric Froude Number

$$Fr_d = \frac{U}{\sqrt{Rcgh}} \quad (1)$$

where  $U$  = layer-averaged flow velocity,  $h$  = current thickness,  $g$  = acceleration due to gravity,

$c$  = layer-averaged volume concentration, and  $R = (\rho_s/\rho - 1)$  where  $\rho_s$  denotes the density of sediment and  $\rho$  denotes the density of water. In the present experiments  $c \ll 1$ , so that the suspensions were dilute. A supercritical density underflow is one for which  $Fr_d > 1$ ; such flows vigorously entrain ambient fluid from above (e.g. Turner, 1973). A subcritical density underflow is one for which  $Fr_d < 1$ ; such flows entrain very little ambient fluid. In the case of ponded turbidity currents,  $Fr_d \ll 1$  and the entrainment of ambient fluid essentially drops to zero.

Lamb *et al.* (2004) recently investigated continuous, or sustained, as well as surge-like turbidity currents in a scaled physical model of a minibasin. They observed that for ponded sustained turbidity currents in intraslope basins a relatively sharp interface separated the ponded turbidity current below from the ambient clear water above. Figure 1A shows the head of one of the turbidity currents described in Lamb *et al.* (2004) as it approached the downstream lip of the model minibasin. The Kelvin–Helmholtz billows along the upper surface of the turbidity current characterize the turbulent deformation along this boundary (Allen, 1971; Britter & Simpson, 1978). However, this is not the only possible configuration of the interface between the turbidity current and the clear water above. Figure 1B shows the same turbidity current after the head reached the downstream lip, ponded against it, and formed an upstream-migrating bore that stabilized beyond the left-hand side of the image, resulting in a ponded turbidity current. After ponding, the interface between the turbidity current and the

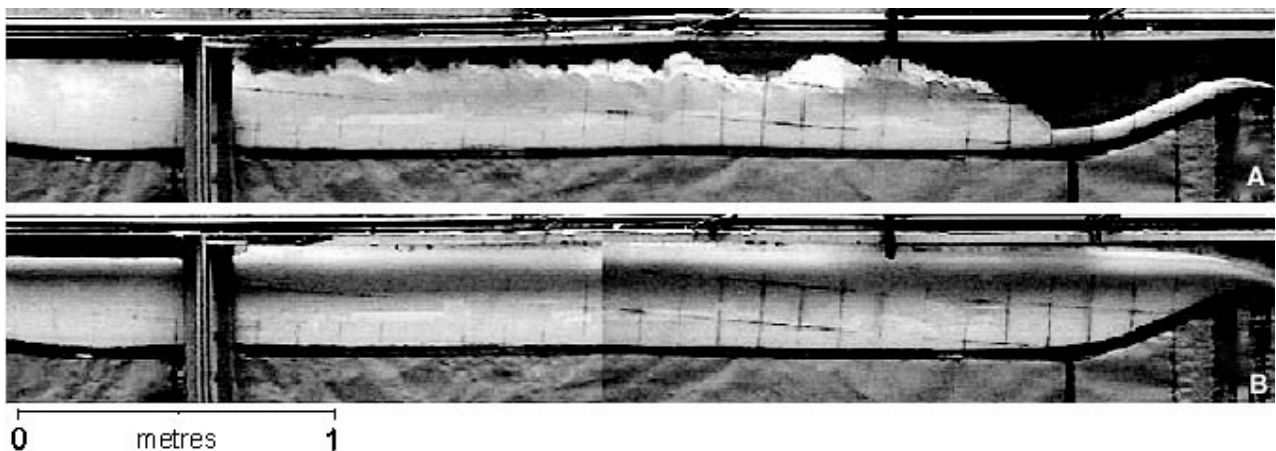


**Fig. 1.** (A) Photograph showing a sustained turbidity current entering the experimental minibasin from the left. Note the turbulent head at the front of the turbidity current. (B) Photograph taken minutes later showing the same turbidity current after the set-up of a quasi-steady ponded turbidity current with a glassy settling interface. The turbidity current is submerged in ambient clear water to an elevation above the top of the figure. The inlet zone is not shown in the image. Figure from Lamb *et al.* (2004) printed with permission of SEPM (Society for Sedimentary Geology).

clear water above became smooth and glassy, indicating highly subcritical flow with virtually no entrainment of ambient clear water into the turbidity current. It is important to emphasize that the input discharge did not change from Fig. 1A to Fig. 1B; the turbidity current was still flowing from left to right.

In this paper, a simple theoretical model is formulated to predict the trapping efficiency of minibasins that pond sustained turbidity currents, and this model is validated against new laboratory experiments reported here as well as those of Lamb *et al.* (2004). The trapping efficiency is defined as the amount of sediment captured in the basin at the end of the flow event divided by the amount of sediment that entered the basin during the flow event. The model shows a limiting case for which a basin traps 100% of the sediment from turbidity currents, even for successive sustained turbidity currents, until deposition within the minibasin is sufficient to force overflow of the turbidity current at the downstream lip. Upscaling suggests that this limiting case can often be expected at the scale of natural minibasins.

The two experiments reported here, while similar to some of the experiments reported in Lamb *et al.* (2004), differ in that (1) the experiments here were designed to achieve much higher sediment trapping efficiencies (i.e. > 95% in the present experiments versus 14–32% in Lamb *et al.* (2004), and (2) the experiments reported

here include measurements of concentration and grain-size of the suspended and deposited sediment, measurements that were previously lacking.

## MODEL OF TRAP EFFICIENCY

Here a simple model based on flow continuity in a ponded turbidity current is formulated. It is assumed that the intraslope basin is sufficiently deep and the duration of the flow is sufficiently long for the set-up of a quasi-steady ponded turbidity current (Lamb *et al.*, 2004). It is useful to define two zones of a ponded turbidity current, the *inlet zone* and the *ponded zone* (Fig. 2). The ponded zone is a region of slow-moving, highly subcritical flow with a distinct glassy horizontal interface separating the turbid flow from the clear water above (e.g. Fig. 1B). In the ponded zone the turbidity current below the interface has little obvious internal structure. Upstream of the ponded zone is an inlet zone. In present experiments the initial inlet flow was subcritical as shown in Fig. 2, resulting in a drowned jet that dissipated farther downstream. When the inlet flow is supercritical, an internal hydraulic jump defines the boundary between the inlet and ponded zones (García, 1993; Toniolo, 2002). The overflow zone near the downstream basin lip (if it exists) should not be considered to be part of the ponded zone, because the turbid water acceler-

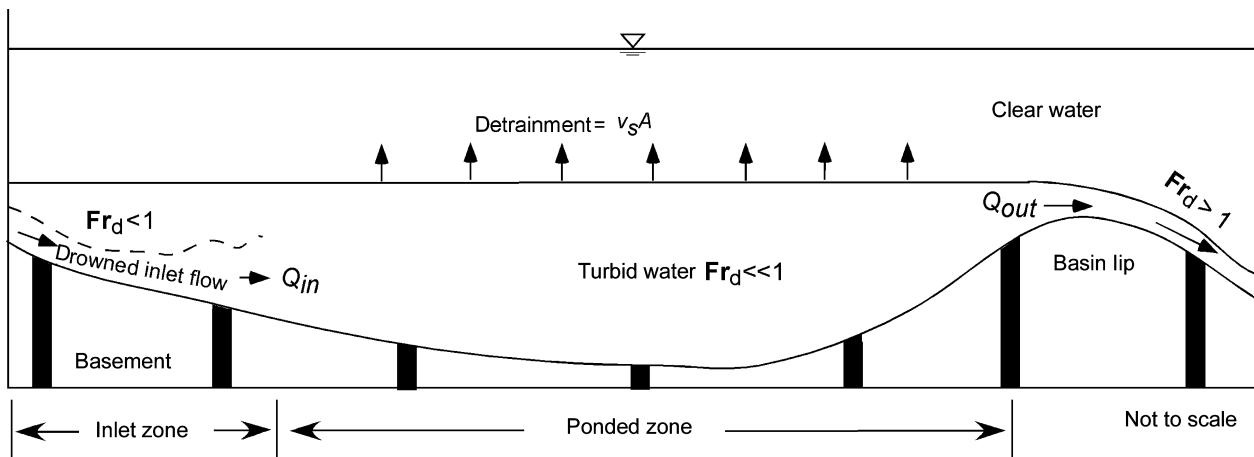


**Fig. 2.** Schematic diagram of an idealized sustained turbidity current after set-up of ponded flow.  $Q_{in}$  is the discharge of turbid water entering the ponded zone and  $Q_{out}$  is the discharge of turbid water out of the ponded zone. As shown, and as was the case at least initially in the experiments, the ponded turbidity current drowns the head gate, creating a drowned underflow ( $Fr_d < 1$ ) in the inlet zone. Note that with supercritical inflow ( $Fr_d > 1$ ), an internal hydraulic jump would define the boundary between the inlet and ponded zones. In the ponded zone, the turbidity current is highly subcritical ( $Fr_d \ll 1$ ) and detraines water across a setting interface at the rate  $v_s A$ , where  $v_s$  is the settling velocity of the sediment and  $A$  is the surface area of the ponded zone. The turbidity current is critical ( $Fr_d = 1$ ) at the lip of the basin and becomes supercritical as it accelerates out of the basin.

ates over the lip and out of the basin (Fig. 2). This results in a critical Froude number at the basin lip, as is expected at an overflow point (Henderson, 1966; Turner, 1973).

Consider first the case of a turbidity current carrying sediment with uniform size  $D$ . The interface between the ponded zone of the flow and the clear water above defines a quasi-steady settling interface through which water is detrained from the turbidity current at the rate  $v_s A$ , where  $v_s$  is the fall velocity of the sediment and  $A$  is the surface area of the ponded zone. That is, if inflow to the ponded zone were stopped, the elevation of the interface would fall at speed  $v_s$ , so converting turbid water to clear water at the volumetric rate  $v_s A$ . The settling interface, however, did not fall in time in the present experiments because turbid water was continuously added to the ponded zone from the inlet. As a result, the position of the settling interface stabilized in time.

Let the volume discharge of sediment-laden flow entering the ponded zone of the minibasin be  $Q_{in}$  and the volume discharge of sediment-laden flow overspilling the downstream basin lip be  $Q_{out}$ . As shown in Fig. 2, flow continuity in the ponded zone requires that

$$Q_{out} = Q_{in} - v_s A. \quad (2)$$

One possibility predicted by this model is that the surface area  $A$  of the ponded zone is sufficient to cause complete detrainment of the inflowing water across the settling interface. In such a case, as long as the interface stabilizes below the level of the downstream lip, no turbidity current overflows the basin resulting in a trapping efficiency of 100%.

In the case of dilute suspensions of sediment mixtures, each grain-size can be expected to develop its own settling interface, so that the interface for sufficiently coarse sediment may be below the lip (with 100% trapping of such sizes) and the interface for sufficiently fine sediment may be above the lip (with <100% trapping of such sizes). Here the above formulation is adapted for mixtures using the Stokes (1851) relation for the settling velocity of sufficiently fine grains:

$$v_s = \frac{1}{18} \frac{RgD^2}{\nu} \quad (3)$$

where  $\nu$  is the kinematic viscosity of the fluid. For natural sediments ( $R \approx 1.65$ ) falling in water ( $\nu \approx 1 \times 10^{-6} \text{ m}^2 \text{ s}^{-1}$ ), the Stokes relation provides a reasonably accurate formulation for

grain-size up to about  $100 \mu\text{m}$  (Dietrich, 1982). The finest size for which 100% trapping can be expected, i.e. the cut-off size  $D_c$ , is the one for which Eq. 2, combined with the given inflow discharge  $Q_{in}$ , the surface area of ponding  $A$ , and Eq. 3, yields an outflow rate  $Q_{out}$  of zero. Thus, if the input grain-size distribution is known, a lower bound on the percentage of mass trapped in the basin (i.e. the trapping efficiency) can be estimated as the mass percentage of the incoming sediment that is coarser than  $D_c$ . This is a lower bound because the trap efficiency of material finer than  $D_c$  is not likely to be zero in the case of a ponded turbidity current, even when there is substantial overflow.

The experiments reported here were specifically designed to achieve a very high trapping efficiency based on Eq. 2. The two experiments are very similar except for the grain-size distributions of the inflowing sediment. The sediment mix used in Experiment 1 had a much lower geometric standard distribution of sizes (and modestly lower geometric mean size) than that used in Experiment 2. The experiments thus allow the effect of the grain-size distribution on the trapping efficiency of minibasins to be studied.

## EXPERIMENTAL SET-UP

The experimental flume used for the present experiments (Fig. 3) was the same flume used and described in detail by Lamb *et al.* (2004) and Toniolo (2002). The installed model minibasin was scaled through an analysis of 13 minibasins from the Gulf of Mexico (Lamb *et al.*, 2004). The width of the minibasin was 0.31 m, and the length from the inlet to the downstream lip was 4.10 m.

Two experiments were completed with approximately the same input discharge and sediment concentration (Table 1). For Experiment 1, a well-sorted sediment consisting of glass beads (ballotini; density  $\rho_s = 2500 \text{ kg m}^{-3}$ ), with a geometric mean grain-size  $D_g$  of  $41 \mu\text{m}$  and a geometric standard deviation  $\sigma_g$  of 1.28, was used to approximate uniform sediment. For Experiment 2, a more poorly sorted silica flour ( $\rho_s = 2650 \text{ kg m}^{-3}$ ), with  $D_g = 53 \mu\text{m}$  and  $\sigma_g = 1.63$ , was used to create a turbidity current consisting of multiple grain-sizes. The inflowing turbidity currents were mixed in a head tank to a 5% sediment concentration by volume, and then were fed into the flume at a steady flow rate for

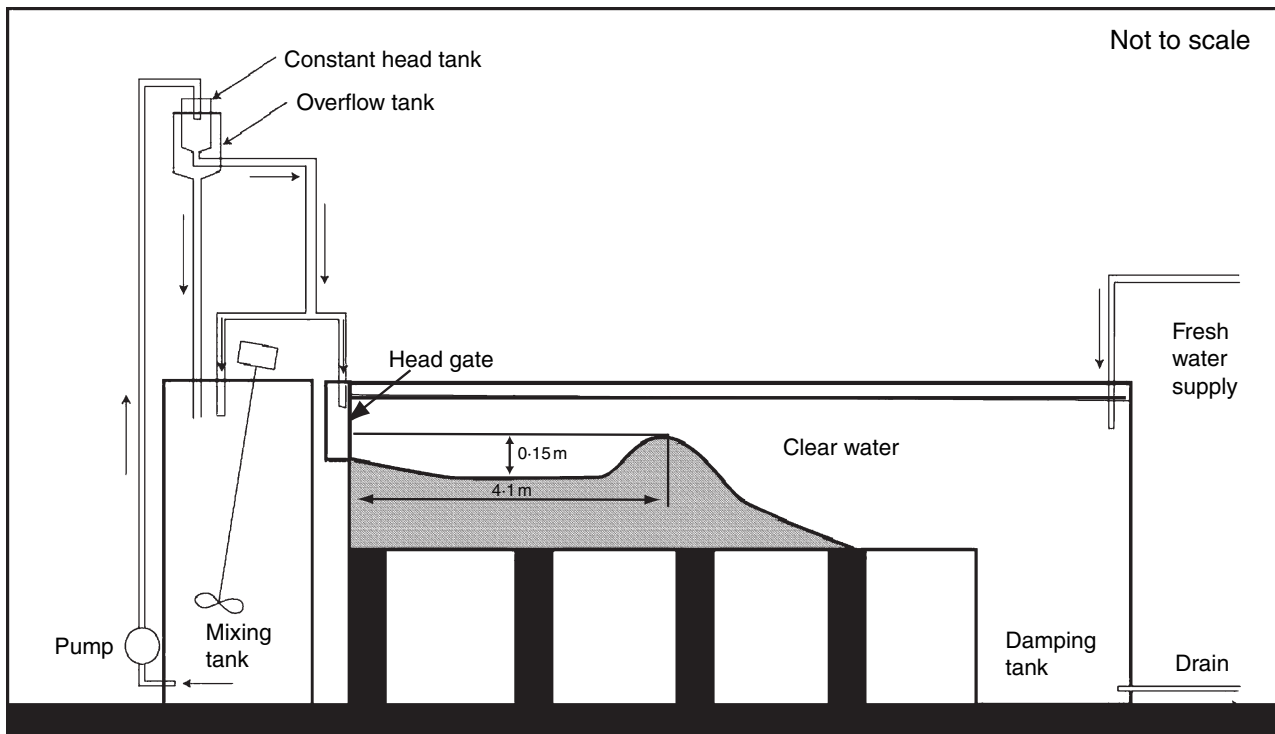


**Fig. 3.** Schematic of the experimental flume. The sediment was kept in suspension in the mixing tank and pumped to a constant head tank in order to maintain a constant sediment concentration and flow rate in the flume. Any turbid water that reached the end of the flume was vented out of the system from a bottom drain in the damping tank. The width of the flume was 0.31 m. Figure reproduced from Lamb *et al.* (2004) with permission of SEPM (Society for Sedimentary Geology).

**Table 1.** Measured and calculated flow characteristics for both the experiments at the entrance head gate and at the basin lip.

	Experiment 1			Experiment 2		
	Mean	$\sigma$	$n$	Mean	$\sigma$	$n$
<b>Head gate</b>						
$Q$ ( $\text{l s}^{-1}$ )	0.26	0.014	3	0.21	0.028	3
$c$	0.05	0.003	2	0.047	0.003	2
$Fr_d$	0.15			0.19		
<b>Basin lip</b>						
$U$ ( $\text{cm s}^{-1}$ )	1.33	0.33	3	3.03	0.63	4
$h$ (cm)	6.07	1.61	3	3.38	0.65	4
$c$	0.00048	0.00035	3	0.0017	0.0012	3
$Fr_d$	1.00			0.62		

The mean, standard deviation ( $\sigma$ ), and the sample size ( $n$ ) are given for the measured values of discharge ( $Q$ ), volumetric concentration ( $c$ ), flow velocity ( $U$ ), and flow height ( $h$ ). The densimetric Froude number ( $Fr_d$ ) was calculated from these values. Note that  $c$  and  $U$  were measured such that they represent cross-sectional averaged values, except for  $c$  at the basin lip, which was measured at 1.4 cm above the bed for both experiments.

approximately 80 min. The turbidity currents were released from a submerged head gate, constricting the initial flow depth to 3 cm and flow width to the width of the flume, resulting, at least initially, in subcritical inlet flow (Fig. 3). The bottom of the head gate was flush with an inerodible channel bed. The elevation of the settling interface was tracked visually through the glass walls of the flume during both the experiments. In addition, the boundary between the ponded and inlet zones was estimated by inserting dye into the inlet flow and visually approximating the streamwise location where the dye became mixed in the vertical.

During the experiments, siphon samples of the flow ( $\sim 250$  ml) were taken at three intervals in time. The first set of measurements was taken between 15 and 25 min, the second set between 35 and 45 min, and the third set between 60 and 70 min after experiment commencement. Three rakes of siphons, each consisting of five vertically stacked siphons, were used in order to sample each turbidity current at three locations in the streamwise direction. The siphons were lowered

into the flow from carts mounted on top of the flume. The samples were later analysed for sediment concentration and grain-size. Sediment concentration was measured by weighing and drying the flow samples. The grain-size distributions of the sediment were then measured with an Elzone particle analyser. Since all of the samples were taken well after the time needed for set-up of quasi-steady ponded flow [ $\sim 1$  min (Lamb *et al.*, 2004)], there was little temporal change in sediment concentration and grain-size. Therefore, the temporal-average of the measurements at each position are presented along with the temporal standard deviation.

Coal powder was fed into the basin immediately after the flow samples were taken in order to record the elevation of the sediment bed at the end of each measurement interval, and to allow for the flow samples to be correlated with bed samples. After each experiment, the resultant deposit was sampled with siphons at three positions in the vertical using the coal markers as bounds, and 4–9 streamwise positions. Each sample was analysed using an Elzone particle analyser to determine the grain-size distribution. Since the flow was quasi-steady with respect to sediment concentration, there was little vertical variation in the grain-size of the deposits. Therefore, the depth-averaged grain-size of the deposit at each streamwise sampling position is presented.

Sediment concentration measurements of the turbid flow overpassing the downstream lip of the basin were compromised in both the experiments because the siphon rake was placed too close to the sediment bed. Both the experiments, however, were repeated using identical parameters in order to resample the turbid flow overpassing the lip of the basin. These repeat experiments had durations of only 30 min as compared to 80 min for the first experiments. However, once the flow stabilized in each experiment very little change in the flow was observed except for gradual aggradation of the bed and rise in the settling interface. In the repeat experiments, the sediment concentration in the turbid flow overpassing the lip of the minibasin was measured with one siphon placed at the apex of the downstream lip, laterally in the middle of the flume, and at 1.4 cm above the bed.

Velocity measurements were attempted using 3 mm Shinozuka micropropellers. In all cases, the velocity of the flow was below the resolution limit of the micropropellers ( $3.5 \text{ cm s}^{-1}$ ). Therefore, visual tracers (neutrally buoyant beads) were

used to estimate the velocity of the turbidity current overflowing the lip of the basin.

## EXPERIMENTAL RESULTS

Upon the commencement of each experiment the head of the inflowing turbidity current traversed the basin, partially reflected off of the downstream lip of the basin, and formed an upstream migrating bore that stabilized near the inlet, drowning the inlet in the process. The turbidity current only partially reflected because a small portion of the head of the turbidity current had enough momentum to flow over the downstream lip and out of the basin. This entire sequence required about 1 min, so establishing a subsequent sustained, quasi-steady, ponded turbidity current. The ponded flow consisted of a sub-critical inlet zone (Table 1) with a persistent underflow (Fig. 4A), and a ponded zone with little internal structure up to a distinct horizontal interface separating the flow from the clear water above (Fig. 4B). The settling interface stabilized at an elevation slightly above the downstream lip of the basin for both the experiments (Fig. 5) resulting in overflow (Fig. 4C). The settling interface rose gradually in time, for a total increase in elevation of 1–2 cm over the duration of each experiment. This was not due to unsteadiness in the inflow, but rather to the steady deposition of sediment on the bed. The depth of clear water above the settling interface was between 20 and 25 cm.

In each experiment vertical profiles of suspended-sediment concentration and grain-size were measured from siphon rake samples at each of three locations, proximal Position 1, medial Position 2, and distal Position 3. The locations of each of these positions for each of the three sample times are given in Fig. 5A for Experiment 1 and Fig. 5B for Experiment 2.

### Inlet zone

Suspended sediment samples were taken in the inlet zone only for Experiment 1, at Position 1 (Fig. 6A). In the inlet zone, there was a notable decrease in sediment concentration and a lesser but still observable decrease in geometric mean grain-size (Fig. 6C) with increasing elevation above the bed. The concentration and grain-size profiles in the inlet zone had a concave-up shape, which is typical in turbulent boundary layer flow (e.g. García, 1994).

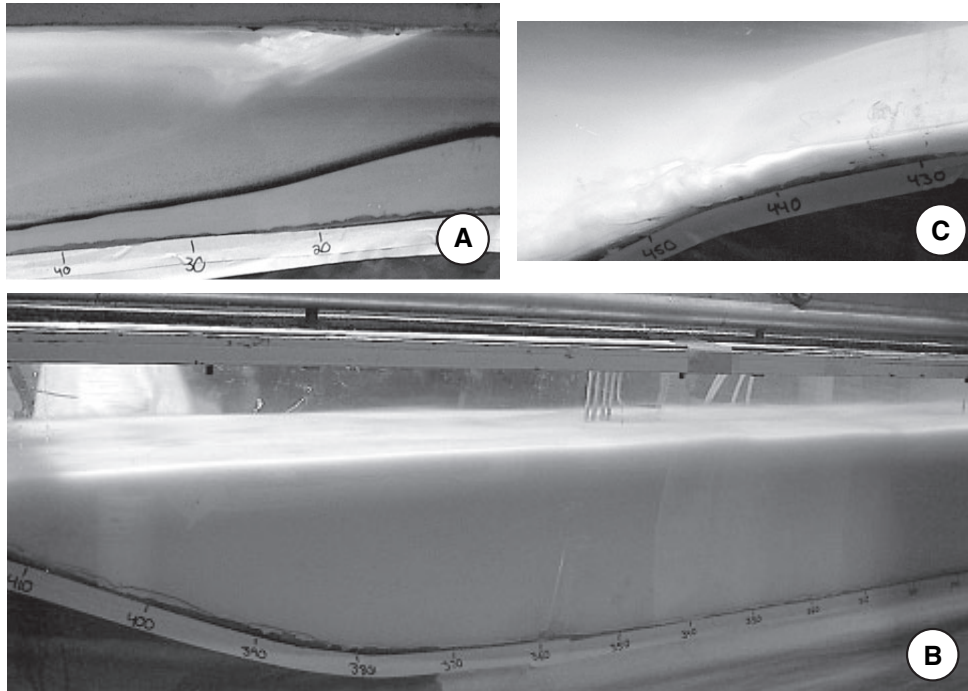


**Fig. 4.** Photographs from Experiment 2 after the set-up of quasi-steady ponded flow. Flow direction is from right to left and the scale along the flume bed is in centimeters. (A) Photograph of the inlet zone from approximately 5 to 45 cm from the head gate showing mixing between the bottom inlet current and the turbid water above. (B) Photograph of the ponded zone from approximately 3 to 4 m from the head gate showing the glassy settling interface. Note that the fluid above the interface was sediment-free water not air. A rake of siphons used to sample the flow is also shown in the image. (C) Photograph of turbid flow going over the basin lip from approximately 4.3 to 4.6 m from the head gate.

In both Experiments 1 and 2, the deposits in the inlet zone were asymmetrical, thinning away from the source (Fig. 5). For Experiment 2, the poorly sorted sediment led to a smaller inlet zone and a more wedge-shaped and coarser-grained deposit with stronger downstream fining of the geometric mean size of the deposit (Fig. 7).

### Ponded zone

In contrast to flow in the inlet zone, the sediment concentration and geometric mean grain-size of the suspended sediment were relatively constant both laterally and vertically in the lower 10 cm of the flow in the ponded zone (Fig. 6). Measurements were taken in the ponded zone for Experiment 1 at Positions 2 and 3, and for Experiment 2 at Positions 1, 2 and 3. The uppermost siphon samples at each position showed a significant drop in sediment concentration, which is consistent with an elevation near the settling interface where the sediment concentration should tend to zero. In addition, concentration decrease in the vertical probably reflects the tendency for coarser size particles to form a lower settling interface.

However, the vertical distribution of suspended sediment in the ponded zone created a convex-up concentration profile confirming that the turbidity currents were better mixed in the ponded zone than in the inlet zone, at least for Experiment 1. In Experiment 2, the more poorly sorted sediment led to higher sediment concentration and slightly finer sediment in the ponded zone, as compared to Experiment 1.

In comparison to the deposits in the inlet zone, the deposits in the ponded zone were finer grained and had a more uniform geometric mean grain-size (Fig. 7) and thickness (Fig. 5). Due to the wider grain-size distribution used in Experiment 2, the downstream variation in geometric mean grain-size of the deposit was more pronounced than that of Experiment 1, but still showed only weak downstream fining.

### Basin lip

The basin lip served as a control point with  $Fr_d \sim 1$  (Table 1), as expected. Due to differences in settling velocities, the sediment in the ponded zone was sorted vertically such that turbid over-

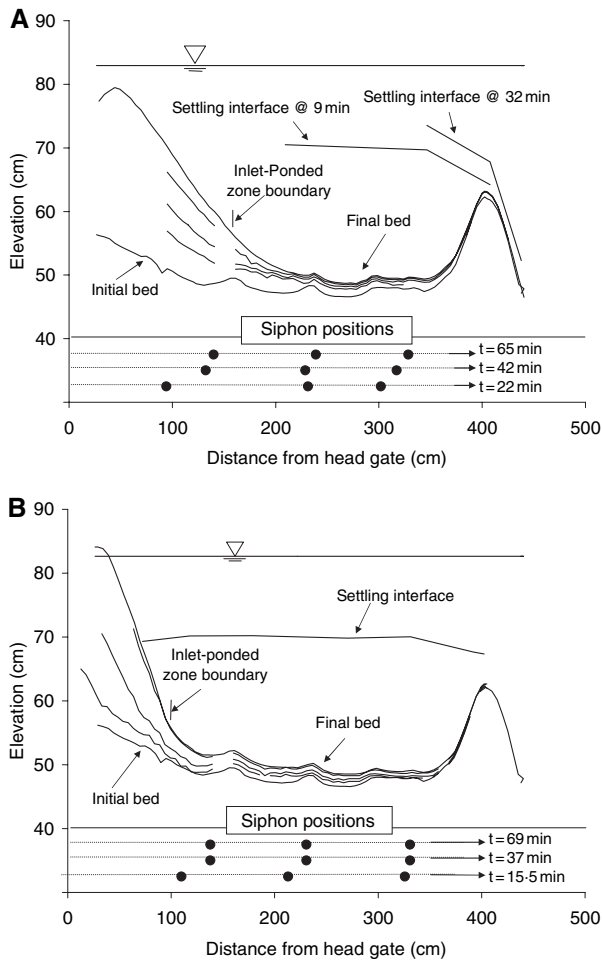


**Fig. 5.** Elevation measurements and streamwise positions of the siphon rakes for (A) Experiment 1 and (B) Experiment 2. The flow was from left to right. Each dot below the elevation profile represents the streamwise position of a siphon rake during the measurement interval denoted by  $t$  in minutes. The proximal, medial, and distal positions at time  $t$  are referred to as Positions 1, 2, and 3, respectively, in the text. In both the figures the elevation of the initial bed, the elevation of the sediment bed during the three measurement intervals, and the elevation of the final sediment bed are shown, as well as the approximate positions of the free surface, the settling interface, and the boundary between the inlet zone and the ponded zone. All of the siphon rakes were in the ponded zone except for the rake at Position 1 during Experiment 1, which was in the inlet zone.

flow was significantly finer than the input sediment (Fig. 8). The overflow samples had  $D_g$  of approximately 22 and 10  $\mu\text{m}$  for Experiments 1 and 2, respectively, as compared to  $D_g$  of the input sediment of 41 and 53  $\mu\text{m}$ , respectively. In addition, the overflow concentration (Table 1) was lower than that measured in the lower part of the ponded zone, by about a factor of six in

Experiment 1 and a factor of three in Experiment 2.

### Trapping efficiency

The sediment concentration, flow velocity, and flow height measurements at the downstream lip of the basin (Table 1) were used to calculate the flux of sediment out of the basin, which when compared to the influx of sediment, resulted in an estimate of sediment trapping efficiency  $T_e$ . The sediment trapping efficiency of the minibasin was 99.1% for Experiment 1 and 95% for Experiment 2. Even though the sediment overflowing the lip of the basin was coarser for Experiment 1, the concentration was so low that the trapping efficiency was nearly 100%. Secondary calculations were done by drying and weighing the sediment deposited within the minibasin after each experiment, so yielding trapping efficiencies of 91.3% and 80.2% for Experiments 1 and 2, respectively. These latter estimates are lower bounds because sediment was lost while draining the flume and weighing the sediment.

### MODEL COMPARISON

Following the model presented above, a lower bound on the trapping efficiency of the basin was predicted for the two experiments reported here, as well as for the continuous flows of Lamb *et al.* (2004). For simplicity, the discharge  $Q_{in}$  entering the ponded zone was approximated as the inlet discharge  $Q$  of Table 1, and the area  $A$  of the ponded zone was approximated as the surface area from the inlet to the downstream lip of the basin shown in Fig. 3. For a channel width of 0.31 m and a length from inlet to downstream lip of 4.1 m, the resulting value of  $A$  is 1.27  $\text{m}^2$ .

Between Eqs 2 and 3, it is found that the cut-off grain-size  $D_c$  that yields a vanishing outflow discharge is given by the relation

$$D_c = \sqrt{\frac{18Q_{in}v}{RgA}}. \quad (4)$$

Water detrainment should thus prevent sediment sizes in excess of the cut-off value  $D_c$  from escaping the basin. A lower bound on basin trap efficiency is then given by the fraction of the incoming sediment that is coarser than  $D_c$ . As discussed above, this is a lower bound because at least some of the sediment finer than the cut-off size can be expected to be trapped in the basin. In

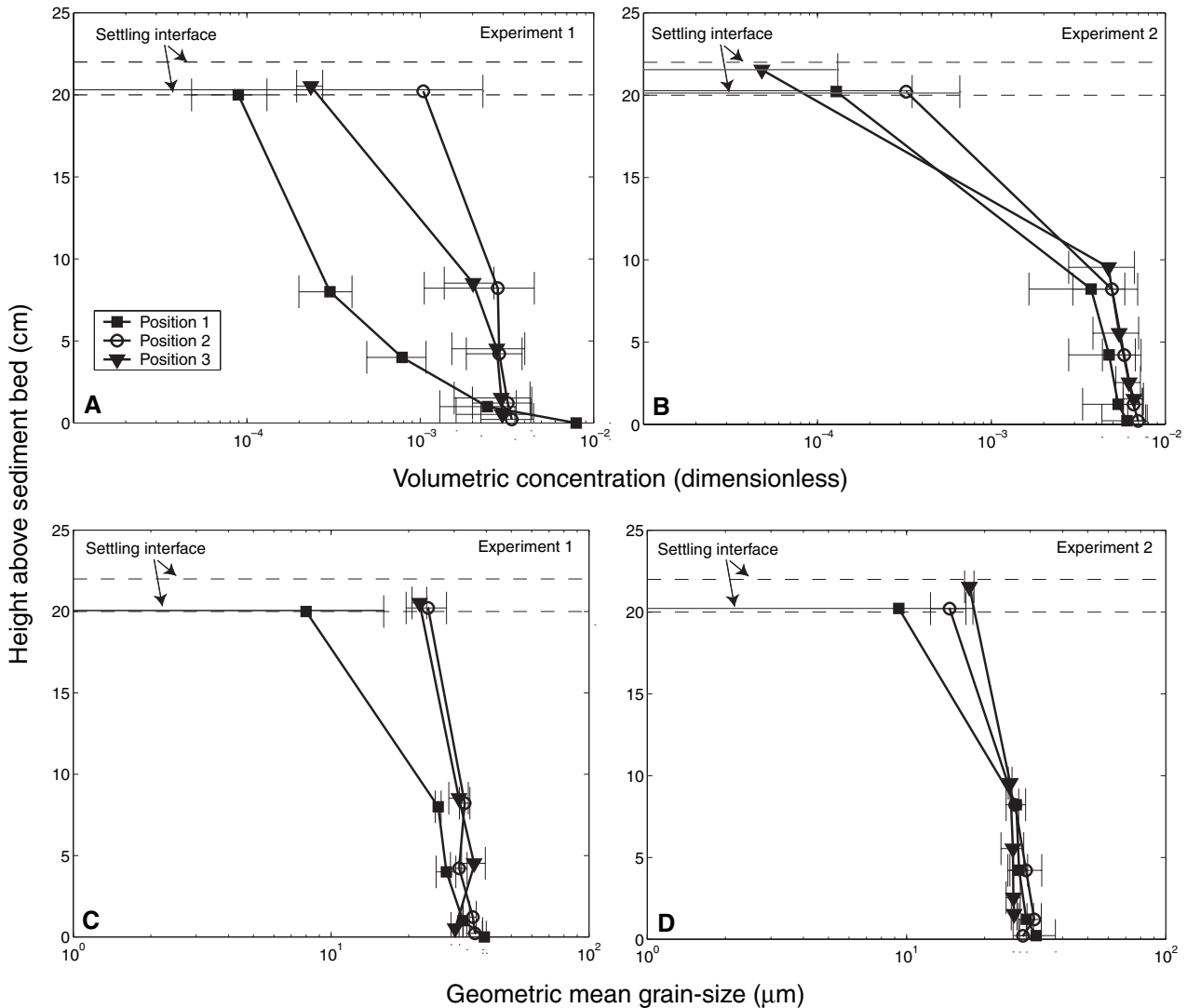


**Fig. 6.** Semilog vertical concentration profiles of the turbidity currents from (A) Experiment 1 and (B) Experiment 2, and semilog vertical profiles of geometric mean grain-size from (C) Experiment 1 and (D) Experiment 2. Each point represents the temporal-average of three samples taken at approximately the same position but at different times during the experiments. The error bars represent  $\pm 1$  SD (temporal) of these measurements. For some points in the region of the settling interface, the measured sediment concentration and grain-size were so small that the error bars extend off of the graph. The three profiles shown in each figure are the measurements taken at three different positions from the head gate. Position 1 corresponds to the samples taken closest to the head gate. Likewise, Position 2 is the middle position, and Position 3 is the distal position. The location of these flow sample positions are shown relative to the basin geometry in Fig. 5. Because the local bed elevation was used as a datum, the elevation of the setting interface was slightly different for each profile. Therefore, an approximate range of the visualized settling interface is shown by the two horizontal dashed lines for each profile.

performing the calculation, the kinematic viscosity of the fluid was set equal to the value for clear water at 20 °C,  $1 \times 10^{-6} \text{ m}^2 \text{ s}^{-1}$ .

The predicted values of  $D_c$  are shown in Table 2. In the case of the two experiments reported here, these values were used in conjunction with the grain-size distributions of Fig. 8 to compute the lower bound on trapping efficiency for each experiment. Grain-size distribu-

tions were not measured for the experiments of Lamb *et al.* (2004). As a result, size distributions of the sediment used in those experiments were acquired directly from the sediment supplier (US Silica Company). The predicted lower bounds on trapping efficiency are showed together with the trapping efficiency calculated from measured values in Table 2 and Fig. 9. The comparison is quite favourable despite the simplicity of the

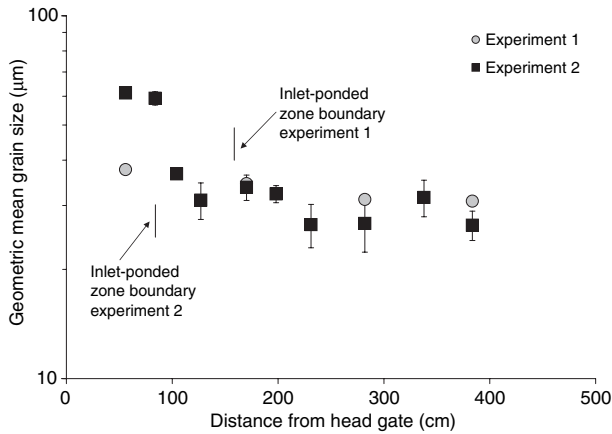


**Fig. 7.** Log-linear plot of the geometric mean grain-size from samples taken of the deposits from Experiments 1 and 2. Three samples were taken at each stream-wise location corresponding to the three stratigraphic intervals that were bounded by coal markers laid down at the end of each interval of flow sampling (Fig. 5). The mean of these three samples is shown and the error bars represent  $\pm 1$  SD. For Experiment 1, the error bars are smaller than the data points. The approximate location of the boundary between the inlet and ponded zones also is shown for both the experiments.

model. In most cases, however, the predicted lower bound on trapping efficiency is slightly higher than the measured trapping efficiency.

The grain-size distributions of the turbid water that overflowed the downstream basin lip and of the deposit can also be used to test the model. The model predicts that all of the sediment that overflows a basin should be finer than  $D_c$ .

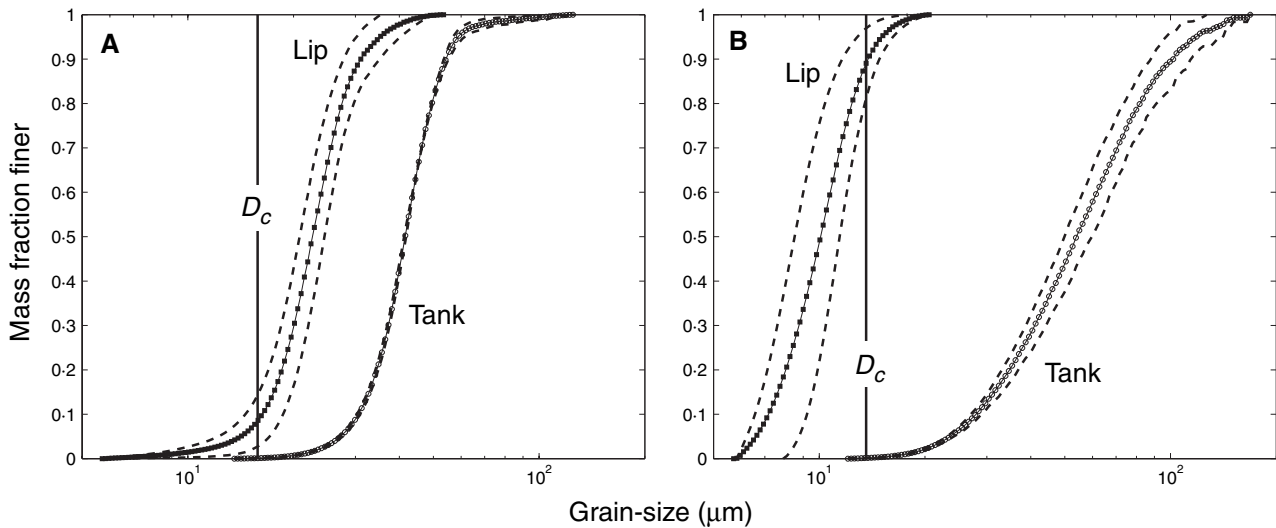


**Fig. 8.** Grain-size distributions of samples from flow entering the minibasin taken from the inlet mixing tank (*Tank*) and samples of the turbid flow overflowing the minibasin at the downstream lip (*Lip*). Three flow samples were taken at each of these locations at different times during an experiment. The data points represent the mean of these three samples and the dashed lines are  $\pm 1$  SD. The predicted maximum basin overflow grain-size ( $D_c$ ) is also shown.

**Table 2.** Input flow discharge ( $Q$ ), input geometric mean grain-size ( $D_g$ ), calculated critical grain-size for minibasin trapping ( $D_c$ ), and the predicted lower bound and measured trapping efficiencies ( $T_e$ ) of the minibasin for the four continuous turbidity experiments of Lamb *et al.* (2004, c1–c4) and the two experiments (E1 and E2) reported in this paper.

	c1	c2	c3	c4	E1	E2
$Q$ ( $l\ s^{-1}$ )	0.5	0.85	2	1	0.26	0.21
$D_g$ ( $\mu m$ )	11	11	11	22	41	53
$D_c$ ( $\mu m$ )	21	27	42	30	16	14
Predicted $T_e$ (%)	26	21.5	12.5	35	99.9	97
Calculated $T_e$ (%)	15	17	14	32	99.1	95

Approximately 90% of the sediment that overflowed the basin lip was finer than  $D_c$  for Experiment 2 (Fig. 8B). For Experiment 1, however, the sediment that passed over the basin lip was mostly coarser than  $D_c$  (Fig. 8A). This was because the well-sorted sediment used in Experiment 1 had almost no grains finer than  $D_c$ . Despite the overflow of sediment coarser than  $D_c$  in Experiment 1, the concentration of these grains was so small that the overflow can be taken as negligible as shown by the 99.1% sediment trapping efficiency. The overflow of sediment coarser than  $D_c$  in both the experiments is consistent with the slight over-prediction of the lower bound on sediment trapping efficiency. The mean grain-size of the sediment captured within the basin (Fig. 7) was significantly coarser than  $D_c$  for both the experiments, as expected.

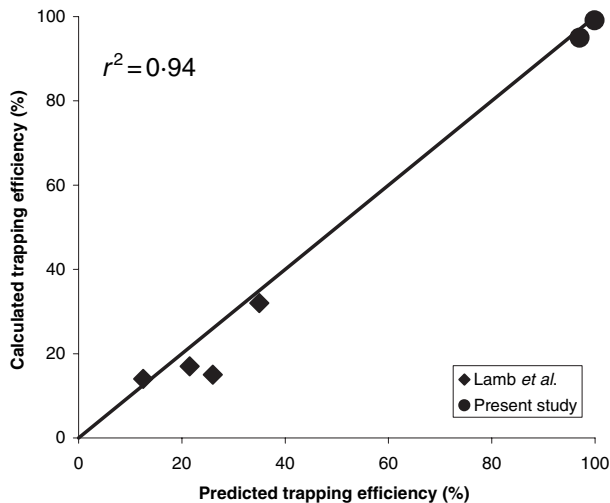


Fig. 9. Predicted lower bound and calculated sediment trapping efficiency for Experiments 1 and 2 as well as the four continuous experiments of Lamb *et al.* (2004).

### IMPLICATIONS FOR NATURAL FLOWS

A typical Gulf of Mexico minibasin has a surface area of 100 km<sup>2</sup> (Lamb *et al.*, 2004). A turbidity current containing exclusively sediment 100 µm in diameter, which has a settling velocity nearly 7.48 mm s<sup>-1</sup> (Dietrich, 1982), would have a potential detrainment discharge equal to  $v_s A$ , or 748,000 m<sup>3</sup> s<sup>-1</sup>, assuming the ponded zone extends over the basin area. For reference, the highest recorded discharge on the Mississippi River has been estimated as 70,000–80,000 m<sup>3</sup> s<sup>-1</sup> (Barry, 1997). Natural turbidity currents carry a distribution of sediment sizes rather than a single size. The potential detrainment discharge is different for each size. This notwithstanding, a lower bound potential detrainment discharge would be 100,000 m<sup>3</sup> s<sup>-1</sup> for mud flocculated to an equivalent fall velocity of 1 mm s<sup>-1</sup> (Hill, 1998).

Since the magnitude of detrainment at natural scales is very large, it seems reasonable that a turbidity current with a flow thickness less than the basin relief should often, if not usually, be completely captured within an intraslope basin. In such a case the settling interface would stabilize at a point below the downstream lip of the minibasin, so causing the capture of 100% of the incoming sediment, even when subjected to a succession of sustained flow events. Overflow must eventually occur, but only as bed aggradation from deposition, by turbidity currents or other mass-transport processes, slowly raises the settling interface to a height above the downstream lip. Deposition within the minibasin

reduces the basin relief and thus gradually reduces the ability of the minibasin to pond incoming turbidity currents.

In present experiments the settling interface of the ponded turbidity current was submerged under 20–25 cm of ambient clear water, whereas in the field it may be submerged under kilometres of water. One necessary condition for the laboratory experiments to provide an accurate model of nature is that the water generated by detrainment induce a negligible flow velocity in the ambient fluid above. Such a condition does not prevail if the depth of submergence of the settling interface below the water surface is too low. However, this was not the case in the present experiments, for which the flow in the ambient water was too slow to be measurable.

It might be argued that scale effects associated with turbulence would give rise to differences in dynamics between the laboratory and natural examples, especially in regard to the transport of suspended sediment. The Reynolds number  $Re$  of the incoming flow can be computed as

$$Re = \frac{Q}{Bv} \quad (5)$$

where  $B$  denotes channel width. The computed values of  $Re$  for Experiments 1 and 2 are 840 and 680, respectively. This suggests a weakly turbulent flow, whereas at natural scales a more turbulent flow might be expected.

However, in a ponded turbidity current, the role of turbulence is irrelevant. Ponding to the point of a very small densimetric Froude number creates a very thick layer of very slow-moving flow. Such a flow is incapable of generating its own turbulence, at either laboratory or natural scale. Any turbulence in the ponded zone must be a relict of the turbulence in the flow upstream of the ponded zone, which should die out in the streamwise direction.

A common misconception is that turbulence somehow *holds* sediment in suspension. However, as long as there is no sediment entrainment at the bed, a patch of suspended sediment falls through a turbulent field at essentially the same rate as if turbulence were absent. Turbulence abets the upward flux of sediment entrained at the bed (and thus balances the downward flux due to fall velocity), but only if there is sediment entrainment at the bed. In a deeply ponded flow, the flow velocities should drop so low that the flow is incapable of re-entraining sediment as it deposits out.

A simple numerical example may be in order. Consider a turbidity current with a discharge of  $100,000 \text{ m}^3 \text{ s}^{-1}$  flowing into a minibasin. Let the ponded flow in the minibasin have a local thickness of 200 m, and a local width of 5000 m. The resulting mean flow velocity is only  $0.10 \text{ m s}^{-1}$ .

Within the ponded zone, then, sediment can be expected to settle out passively, with little or no influence from turbulence. The result is a draped deposit, whether at laboratory or natural scale. Indeed, a draped deposit with only weak streamwise sorting and no evidence of reworking might be the record of a ponded turbidity current. After the cessation of a sustained event, the remnant turbidity current can be expected to form a stagnant settling pond including the finer grains that might have been overflowing the downstream lip during the event. As the sediment settles out and the stagnant pond decays, the draped deposit is probably capped by a thin, finer-grained, normally graded deposit with a ponded geometry (Lamb *et al.*, 2004).

The experiments and the model thus should provide an accurate representation of the dynamics of strongly ponded turbidity currents in nature, as long as their application is limited to the ponded zone. On the other hand, the experiments do not provide a good model of nature in the inlet zone upstream of the ponded zone. In the experiments the minibasin itself is scaled down considerably from natural systems, but sediment sizes are not. As a result, the model flows are not capable of entraining bed sediment to any significant degree. In contrast, natural turbidity currents that are not ponded can freely entrain bed sediment as well as deposit sediment on the bed. Thus, the thick, wedge-shaped deposits in the inlet zone of Fig. 5A and B might be artefacts of the experiments, and cannot be considered to be representative of nature.

## DISCUSSION

Whereas the results for the ponded zone are directly applicable to natural minibasins, the formulation presented here does not represent a complete model of the dynamics of ponded turbidity currents. A more complete model, at least for the case of uniform sediment, is presented in Toniolo (2002). A few relevant points from that work are reproduced here.

It is possible to create a completely ponded turbidity current, with essentially no outflow of

sediment or water as a definable flow over the lip (Toniolo, 2002). In the case of uniform sediment, the flow velocity declines gradually in the streamwise direction to zero at the downstream barrier.

A more realistic model of ponding includes a hydraulic jump at the upstream end of the ponded zone. The location of the hydraulic jump, and thus the area available for detrainment, becomes a rather complex function of barrier height, sediment size and the incoming flow. For a given barrier top elevation, as sediment fills the basin the settling interface rises and the degree of ponding becomes weaker, thus forcing the hydraulic jump downstream and reducing the area available for water detrainment. Eventually the ponded zone can be expected to be largely washed out by deposition, after which time overflow from the downstream lip is substantial. Once this condition is reached, the flow may begin to erode a canyon into the downstream lip.

## CONCLUSIONS

Experiments on sustained turbidity currents filling an intraslope basin have been performed. After the set-up of ponded flow with a steady input discharge, the flow changed little in form, sediment concentration, or grain-size, and so could be considered quasi-steady. The suspended sediment concentration and geometric mean grain-size decreased rather strongly with height above the bed in the inlet zone, where a wedge-shaped deposit displayed strong downstream fining. The use of a more poorly sorted sediment mixture in Experiment 2 (as compared to Experiment 1) resulted in a shorter inlet flow region, and a more strongly wedge-shaped deposit with more pronounced downstream fining in the inlet zone. The sediment concentration profile changed from a concave-up shape in the inlet zone to a convex-up shape in the ponded zone indicating more vertical mixing in the ponded zone. The concentration and geometric mean size of the suspended sediment in the ponded zone varied only weakly in the streamwise direction, resulting in a deposit with a drape-like geometry and only a weak pattern of downstream fining. The more poorly sorted sediment used in Experiment 2 (as compared to Experiment 1) resulted in a higher concentration of and slightly finer suspended sediment in the ponded zone, and more concentrated and finer-grained overflow at the basin lip.

Due to differences in settling velocities, the sediment in the ponded zone was sorted vertically so that only the finer sediment was able to overflow the basin. In both the experiments the settling interface was not far above the downstream lip. As a result, sediment trapping efficiencies were >95%. The ponded turbidity current was separated from the sediment-free fluid above by a horizontal glassy interface, indicating very slow, highly Froude-subcritical flow in the ponded zone. The trapping of sediment within the basin was governed by the relative magnitudes of the input discharge of turbid water and the detrainment discharge of water across this interface. Flow continuity shows a limiting case in which an intraslope basin captures 100% of the sediment from a ponded turbidity current, even over a succession of sustained flows. Upscaling of these arguments suggests that many intraslope minibasins in nature should be effective traps for most of the incoming sediment even from a succession of sustained turbidity currents, at least until such time as deposition within the basin drives the settling interface well above the downstream lip of the basin.

## ACKNOWLEDGEMENTS

This research was supported by the St. Anthony Falls Oil Consortium (Anadarko, ChevronTexaco, ConocoPhillips, ExxonMobil and Japan National Oil Company) and the Office of Naval Research STRATAFORM program (grant to G. Parker). We thank Jeff Marr, Ben Sheets, Nikki Strong and Jake Violet for assisting with the experiments. Chris Paola added significantly through many valuable discussions. Finally, we thank Tom Hickson, whose initial experiments inspired many of the ideas presented in this paper and for providing us with Figs 1 and 3. An earlier version of this paper greatly benefited from reviews by Peter Haughton, Stuart McLelland, and an anonymous reviewer.

## NOMENCLATURE

$A$	surface area of the ponded zone
$B$	channel width
$c$	layer-averaged volumetric sediment concentration
$D$	sediment diameter
$D_c$	finest grain-size for 100% trap efficiency
$D_g$	geometric mean grain-size

$Fr_d$	densimetric Froude number
$g$	acceleration due to gravity
$h$	flow thickness
$n$	number of measurements
$Q$	flow discharge
$Q_{in}$	flow discharge entering the ponded zone of the minibasin
$Q_{out}$	flow discharge spilling over the downstream basin lip
$R$	submerged specific density of sediment
$Re$	Reynolds number
$T_e$	minibasin sediment trapping efficiency
$U$	layer-averaged flow velocity
$\nu$	kinematic viscosity
$v_s$	sediment settling velocity
$\rho$	density of water
$\rho_s$	density of sediment
$\sigma$	standard deviation
$\sigma_g$	geometric standard deviation

## REFERENCES

- Allen, J.R.L.** (1971) Mixing at turbidity current heads, and its geological implications. *J. Sediment. Petrol.*, **41**, 97–113.
- Badalini, G., Kneller, B. and Winker, C.D.** (2000) Architecture and processes in the late Pleistocene Brazos-Trinity Turbidite System, Gulf of Mexico Continental Slope. In: *Deep-Water Reservoirs of the World* (Eds P. Weimer, R.M. Slatt, J. Coleman, N.C. Rosen, H. Nelson, A.H. Bouma, M.J. Styzen and D.T. Lawrence), pp. 16–34. Gulf Coast Section SEPM, Houston, TX.
- Barry, J.M.** (1997) *Rising Tide*. Simon and Schuster, New York, 574 pp.
- Beaubouef, R.T. and Friedmann, S.J.** (2000) High resolution seismic/sequence stratigraphic framework for the evolution of Pleistocene intra slope basins, western Gulf of Mexico: depositional models and reservoir analogs. In: *Deep-Water Reservoirs of the World* (Eds P. Weimer, R.M. Slatt, J. Coleman, N.C. Rosen, H. Nelson, A.H. Bouma, M.J. Styzen and D.T. Lawrence), pp. 40–60. Gulf Coast Section SEPM, Houston, TX.
- Brami, T.R., Pirmez, C., Archie, C. and Holman, K.L.** (2000) Late Pleistocene deep-water stratigraphy and depositional processes, offshore Trinidad and Tobago. In: *Deep-Water Reservoirs of the World* (Eds P. Weimer, R.M. Slatt, J. Coleman, N.C. Rosen, H. Nelson, A.H. Bouma, M.J. Styzen and D.T. Lawrence), pp. 104–115. Gulf Coast Section SEPM, Houston, TX.
- Britter, R.E. and Simpson, J.E.** (1978) Experiments on the dynamics of a gravity current head. *J. Fluid Mech.*, **88**, 223–240.
- Dietrich, W.E.** (1982) Settling velocity of natural particles. *Water Resour. Res.*, **18**, 1615–1626.
- Edwards, D.A.** (1993) *Turbidity Currents: Dynamics, Deposits and Reversals*. Lect. Notes in Earth Sci., vol. 44. Springer-Verlag, Berlin, 173 pp.
- García, M.H.** (1993) Hydraulic jumps in sediment-driven bottom currents. *J. Hydraul. Eng.*, **119**, 1094–1117.
- García, M.H.** (1994) Depositional turbidity currents laden with poorly sorted sediment. *J. Hydraul. Eng.*, **120**, 1240–1263.

- Henderson, F.M.** (1966) *Open Channel Flow*. Macmillan, New York, 522 pp.
- Hill, P.S.** (1998) Controls on floc size in the coastal ocean. *Oceanography*, **11**, 13–18.
- Kneller, B.** and **Buckee, C.** (2000) The structure and fluid mechanics of turbidity currents: a review of some recent studies and their geologic implications. *Sedimentology*, **47**(Suppl. 1), 62–94.
- Kneller, B.C., Edwards, D., McCaffrey, W.** and **Moore, R.** (1991) Oblique reflection of turbidity currents. *Geology*, **19**, 250–252.
- Lamb, M.P., Hickson, T., Marr, J.G., Sheets, B., Paola, C.** and **Parker, G.** (2004) Surging versus continuous turbidity currents: flow dynamics and deposits in an experimental intraslope basin. *J. Sediment. Res.*, **74**, 148–155.
- Pratson, L.F.** and **Ryan, W.B.F.** (1994) Pliocene to recent infilling and subsidence of intraslope basins offshore Louisiana. *Am. Assoc. Pet. Geol. Bull.*, **78**, 1483–1506.
- Rottman, J.W., Simpson, J.E.** and **Hunt, J.C.R.** (1985) Unsteady gravity current flows over obstacles: some observations and analysis related to the Phase II trials. *J. Hazardous Mater.*, **11**, 325–340.
- Schollnberger, E.** and **Vail, P.R.** (1999) Seismic sequence stratigraphy of the lower Congo, Kwanza, and Benguela basins, offshore Angola, Africa. *Am. Assoc. Pet. Geol. Bull.*, **83**, 1338.
- Stokes, G.G.** (1851) On the effect of the internal friction of fluids on the motion of pendulums. *Cambridge Philos. Trans.*, **9**, 8–106. Reprinted in: *Mathematical and Physical Papers* (1966) 2nd edn, Vol. 3, Johnson Reprint Corp., New York.
- Toniolo, H.** (2002) *Debris Flow and Turbidity Current Deposition in the Deep Sea and Reservoirs*. PhD Thesis, University of Minnesota, Minneapolis, 233 pp.
- Turner, J.S.** (1973) *Buoyancy Effects in Fluids*. Cambridge University Press, Cambridge, 367 pp.
- Woods, A.W., Bursik, M.I.** and **Bukatov, A.V.** (1998) The interaction of ash flows with ridges. *Bull. Volcanol.*, **60**, 38–51.

*Manuscript received 4 September 2003; revision accepted 2 August 2005.*